Materials Today Communications 4 (2015) 156–165

Contents lists available at ScienceDirect

Materials Today Communications

journal homepage: www.elsevier.com/locate/mtcomm

Nitrogen-doped porous carbons for highly selective CO_2 capture from flue gases and natural gas upgrading

Jun Wang[a], Rajamani Krishna[b], Jiangfeng Yang[c], Kodanda Phani Raj Dandamudi[a], Shuguang Deng[a,*]

[a] Chemical & Materials Engineering Department, New Mexico State University, Las Cruces, NM 88003, USA
[b] van't Hoff Institute for Molecular Sciences, University of Amsterdam, Science Park 904, 1098 XH Amsterdam, The Netherlands
[c] Research Institute of Special Chemicals Taiyuan, University of Technology, Taiyuan 030024, Shanxi, PR China

ARTICLE INFO

Article history:
Received 18 May 2015
Received in revised form 10 June 2015
Accepted 18 June 2015
Available online 30 June 2015

Keywords:
Nitrogen-doped
Activated carbon
CO_2 capture
Natural-gas upgrading
Breakthrough simulation

ABSTRACT

Nitrogen-doped microporous activated carbon adsorbents were synthesized by a self-template method with KOH as the porogen agent at pyrolysis temperatures of 600, 700, and 800 °C. The carbon adsorbent samples were characterized with N_2 adsorption at 77 K, X-ray diffraction, scanning electron microscopy, transmission electron microscopy, thermal gravimetric analysis, Raman spectroscopy, Fourier transformed infrared spectroscopy, and energy-dispersive X-ray spectroscopy mapping. Single component gas adsorption equilibrium of CO_2, CH_4, and N_2 on the carbon adsorbents were measured at gas pressures up to 100 kPa and temperatures of 273, 298, and 323 K. Adsorption breakthrough performance of a fixed bed packed with the carbon adsorbents for separation of $CO_2/CH_4/N_2$ gas mixture was simulated using the adsorption equilibrium data collected in this work. A high CO_2 adsorption capacity (6.36 mmol g^{-1} on N-AC 600 at 100 kPa and 273 K) and large selectivites for the separation of CO_2/CH_4 (9.2), CO_2/N_2 (47.3) and CH_4/N_2 (3.6) mixtures were achieved with the carbon adsorbents due to their N-containing groups, narrow pore size distribution, and large specific surface area. The nitrogen-doped porous carbon adsorbents look very promising for flue gas treatment and natural gas upgrading applications.

1. Introduction

CO_2 emission from flue gases, originating from power plants burning fossil fuels, contributes significantly to the increase of CO_2 concentration in the atmosphere, which is widely believed to result in the global climate changes. Approximately, 30% of CO_2 emitted to atmosphere comes from fossil fuel based power plants as a result of human activity [1]. Typical flue gases contain about 79% N_2, 17% CO_2 and 4% O_2 [2]. CO_2, in its pure form, is a very useful raw material in industry, such as dry ice, additive in beverages, and feedstock for biomass cultivation. Therefore, there is a need to separate the CO_2 present in flue gases before exhausting into the atmosphere [3,4]. Natural gas is considered as an alternative and cleaner energy sources to replace petroleum and coal. The U.S. consumes ~22 trillion scf/yr (standard cubic feet/year), and the whole world consumes ~95 trillion scf/year [5]. However, the raw natural gas contains undesired impurities of CO_2, N_2, and H_2O, which will corrode pipeline and lower the calorific value. The U.S. pipeline specification for natural gas requires less than 2% CO_2 and 4% N_2. However, the raw natural gas could contain up to 18% of CO_2 and 20% of N_2 [6,7]. All raw natural gas requires a pre-treatment, and ~20% needs an extensive treatment, before being delivered to the pipeline, which makes natural gas upgrading one of the largest gas separation applications.

Several technologies have been investigated for the CO_2 capture and separation, such as membrane [8], cryogenic distillation [9], amine solutions absorption [10], temperature swing adsorption (TSA) [11], and pressure swing adsorption [12]. The selectivity of preferential adsorption of component 1 over component 2 in a mixture containing 1 and 2, perhaps in the presence of other components too, can be formally defined as

$$S_{ads} = \frac{q_1/q_2}{p_1/p_2}$$

In above equation, q_1 and q_2 are the absolute component loadings of the adsorbed phase in the mixture. These component loadings are also termed the uptake capacities. The main technology used in industry for CO_2 capture is simply the amine solution absorption by forming the N—C bonded carbamate [13,14]. However, this technology is very energy intensive primarily because

* Corresponding author.
E-mail address: sdeng@nmsu.edu (S. Deng).

http://dx.doi.org/10.1016/j.mtcomm.2015.06.009
2352-4928/

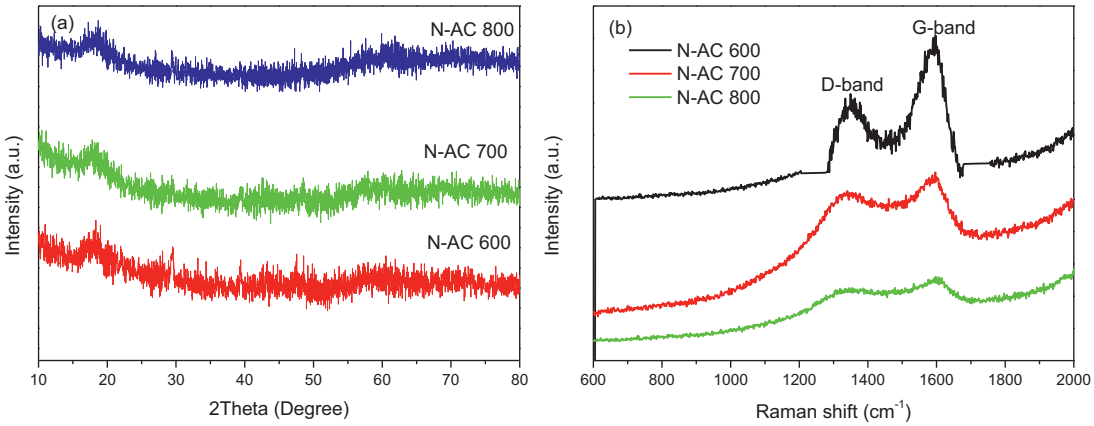

Fig. 1. (a) XRD patterns and (b) Raman spectra of N-AC 600, N-AC 700, and N-AC 800.

of the need for solvent regeneration; it also suffers from corrosion and chemical decomposition [10]. Therefore, we need to find more energy-efficient and environment-friendly alternative solutions for CO_2 capture and separation. Among the existing technologies, adsorption on solid adsorbents is considered a promising future solution [15]. The key to the success of CO_2 capture and natural gas separation by adsorption is to identify porous adsorbent materials that have a high capacity and large selectivity for CO_2/N_2, CH_4/CO_2 and CH_4/N_2 separation.

Synthesis, characterization and evaluation of porous materials for selective adsorption of CO_2 are very popular research endeavors in material chemistry, chemical engineering, environmental science and engineering. Many adsorbents have been applied in capturing CO_2 from flue gases and natural gases upgrading, such as metal-organic frameworks (MOFs) [16,17], hyper-cross-linked polymers (HCPs) [18,19], conjugated microporous polymers (CMPs) [20,21], amine-modified mesoporous silicas [22], and activated carbons (ACs) [23]. Chen et al. reported a highly selective CO_2 adsorbent, MOF-508b with an adsorption capacity of 26.0 wt% at 303 K and 4.5 bar [24]. Py-1, which is an aromatic heterocyclic microporous polymer material, showed high CO_2/N_2 selectivity about 117 at 273 K [25]. One amine-doped mesocelullar silica foam (MSF) has been developed with a remarkably high CO_2 uptake of 4.5 mmol g^{-1} at 248 K and 1 bar [26].

Activated carbon has a promising future in industrial application due to its easy of synthesis, high CO_2 adsorption capacity, excellent selectivity, stability, easy to regenerate, and excellent selectivity over a wide range of operation conditions [27,28]. Nitrogen-doped carbon adsorbent is on the top in this category because of its enhanced interactions between CO_2 and the N-functional groups. Methodology of decorating carbon with nitrogen could be: (i). using inherent N-containing precursors; (ii). pretreating precursors with N-containing additives; (iii). utilizing natural N content in biomass [29]. Uyama et. al reported activated carbon monoliths (ACMs), fabricated by carbonization of polyacrylonitrile, exhibiting a high CO_2 uptake of 5.14 mmol g^{-1} under ambient conditions [30]. NC900, derived from ZIF-8 with NH_4OH as the secondary nitrogen sources, showed a high CO_2 capacity of 5.1 mmol g^{-1} at 273 K and 1 bar [31]. Chitosan derived N-doped microporous carbons demonstrated an excellent CO_2 uptake performance of 3.86 mmol g^{-1} at 298 K and 1 atm, in addition, an extraordinary CO_2/N_2 separation selectivity of 21 was also observed [32].

Polymer template N-doped activated carbon adsorbents are desirable and favorable, because of avoiding extra reaction and efficient doping. In 2012, Chandra et al. [33] demonstrated that a N-doped carbon that was prepared by chemical activation of polypyrole has exhibited a high CO_2 adsorption capacity of 4.3 mmol g^{-1} at 298 K and 1 atm. An ordered N-doped mesoporous carbon prepared through a direct self-assembly of resorcinol-melamine-formaldehyde and F127 has shown an improved CO_2 adsorption of 4.6 mmol g^{-1} at 273 K [34]. A N-doped hierarchical micro-mesopore structure carbon was obtained through a pyrolysis of a porous polymer prepared from terephalaldehyde and melamine, and displayed a CO_2 capacity of 6.3 mmol g^{-1} at 298 K and excellent CO_2/N_2 separation selectivity of 32 [35]. However, this method has several drawbacks such as relatively high cost for the pure chemicals used in the synthesis process, use of hazardous organic solvent, and difficulty in scaling up.The object of this work is to develop a serial of novel self-template N-decorated activated carbons as adsorbents for CO_2 capture and natural gas upgrading. Three pyrolysis temperatures (873, 973, and 1073 K) and one porogen agent (KOH) were applied and compared. The significance of N-content has been discussed in improving CO_2 uptake ability and CO_2/N_2, CO_2/CH_4, and CH_4/N_2 selectivities.

2. Experimental

2.1. Preparation of N-ACs

To synthesize the precursor, 3 g of terephthalaldehyde (TTD) was dispersed in 50 mL dichlorideethane (DCE) at a room temperature under sonication. 8 g of ethylenediamine (EDA) dissolved in 50 mL DCE was added to this solution. 5 g of formic acid was added as a catalyst. The resulting solution was stirred and allowed to polymerize for 24 h at 100 °C. Then raised the temperature to 170 °C, let the polymerization conduct for another 2 days. The resulting polymer is poly(2-phenyl-1,3,6,8-tetraazacyclodecane). The schematic representation of this N-containing network is shown in Fig. S1. After the polymerization, 100 mL methanol was added, and the final mixture was filtered. The obtained yellow precipitate was washed with 500 mL methanol and 500 mL deionized (DI) water. The precipitate was then resuspended in 100 mL 1 M HCl at a room temperature for 3 h. The solution was filtered. The precipitate was washed with DI water until a neutral pH was observed. Finally, the polymer material was dried at 80 °C for 24 h under a vacuum.

The chemical activation of the nitrogen-doped samples was carried out using 1:2 ratio of precursor and potassium hydroxide. Typically, 1.5 g polymer material and 3 g of KOH were added to a molar, and then, ground to produce a uniform light yellow powder. Pyrolysis was carried out by heating the mixture for 1 h in a tube furnace in an nitrogen atmosphere at three different temperatures (600, 700, and 800 °C). The heating rate is 3 °C/min. After activation the carbon product was washed with 8% HCl, then, washed

with 500 mL DI water until a neutral pH was observed. The final precipitate was dried under a vacuum at 80 °C for 24 h.

2.2. X-ray diffraction (XRD)

The XRD pattern was recorded using a Rigaku Miniflex-II X-ray diffractometer with Cu Kα (λ = 1.5406 Å) radiation, 30 kV/15 mA current, and kβ-filter. A step scan with an increment of 0.02° in 2θ and a scan rate of 1°/min was employed to obtain the high-resolution patterns.

2.3. Fourier transformed infrared (FT-IR)

FT-IR spectra were recorded with a PerkinElmer FT-IR/NIR Spectrum 400 using the attenuated total reflectance method (ATR). The spectrum was generated, collected 4 times, and corrected for background noise. Experiments were done on the powder samples.

2.4. Scanning electron microscopy (SEM) & energy dispersive X-ray spectroscopy (EDS)

SEM images and EDS mapping of the materials were taken using SEM S-3400NII equipped with energy-dispersive X-ray analysis (EDS).

2.5. Transmission electron microscopy (TEM)

TEM images were taken by Hitachi H-7650. Raman spectra: Raman spectra were collected using Reinshaw Raman microscope with 632.8 nm (1.96 eV) laser excitation.

2.6. Thermal analysis

Thermogravimetric curves were collected in a PerkinElmer Pyris I thermogravimetric analyzer. The samples (initial or exhausted) were exposed to an increase in temperature of 10 °C/min from 25 to 900 °C under a flow of nitrogen held at 100 mL/min.

2.7. CHNO element analysis

Ultimate Analysis of the carbon samples was performed using an Elemental Analyzer (PE 2400 Series II CHNS/O Analyzer). All the samples were dried to ensure the sample is completely free of water. A sample of 5 ± 1.0 mg was used for measuring the elemental compositions during the analysis. Oxygen values for the samples are calculated by difference O% = 100 − (C + H + N + S)%.

2.8. Adsorption isotherm measurements

The pure component adsorption isotherms of CO_2, CH_4, and N_2 at three temperatures (273, 298, and 323 K) and gas pressure up to 800 mmHg were measured volumetrically in the Micromeritics ASAP 2020 adsorption apparatus. All temperatures were achieved by using a dewar with a circulating jacket connected to a thermostatic bath with a precision of ±0.01 °C. The degas procedure was repeated in all samples before measurements at 250 °C for 24 h. Ultrahigh purity grade CO_2, CH_4, N_2, and He from Matheson Co., were used as received. BET (Brunauer–Emmett–Teller) surface area was calculated between 0.05–0.3 relative pressure and pore size distributions were calculated using NLDFT (Non-Local Density Functional Theory) from N_2 adsorption–desorption isotherms measured at 77 K.

3. Results and discussion

3.1. Material synthesis and characterization

Three nitrogen-doped porous carbon samples N-AC 600, N-AC 700, and N-AC 800 were synthesized at pyrolysis temperatures of 600, 700 and 800C, respectively. The crystallographic structure and molecular morphology of these samples were investigated by XRD and Raman spectroscopy, and the experimental results are shown in Fig. 1. As Fig. 1a shows, XRD patterns of N-AC 600, N-AC 700, and N-AC 800 exhibit one broad diffraction peak centered at around 2θ of 16°, contributed to the (0 0 2) crystal planes of graphitic carbon. We can find that the (0 0 2) peak centered at 2θ of 16° shifts to a lower and lower angle, for N-AC 600, N-AC 700, and N-AC 800, respectively. The intensity of the peak is weak and faintly broadened for N-AC 700 and N-AC 800, compared to that of N-AC 600. This phenomenon reveals a decreased degree of graphitization and crystallinity due to the existence in more graphene fragments and defects on carbon materials with activation temperature increasing [36,37].

The defective nature of nitrogen-doped carbons synthesized at high temperatures can be confirmed by Raman spectra (Fig. 1b). As shown in Fig. 1b, two peaks broad bands at around 1358 and 1588 cm^{-1} can be observed, which correspond to the D and G bands of the carbon, respectively. The D band corresponds to the breath modes of rings or κ-point phonons of A1 g symmetry, while the G band represents the in-plane bond-stretching motion of the pairs of C sp2 atoms (the E2 g phonons) [38,39]. The intensity ratio between D and G bands (I_D/I_G) could exactly reflect the degree of graphitic of carbon materials. The intensity ratio is 0.56, 0.87, and 0.95 for N-AC 600, N-AC 700, and N-AC 800, respectively. The increasing values indicate that N-AC 800 possesses the most defective nature and lowest graphitized degree. This could be attributed to the higher porous and disordered structure caused by a higher activated temperature, which is consistent with the XRD results. FT-IR spectra of all three samples were scanned 4 times at a resolution of 1 cm^{-1}. As shown in Fig. S2, the bands that appear at approximately 1615, 2820, 2870, and 3400 cm^{-1} are contributed to plane N—H bending, aldehydes breathing, methyl stretching, and O-H stretching, respectively. We also noticed that C═O stretching is barely shown in N-AC 800. All carbon samples showed a N-H stretching, indicating that N was introduced into the carbon samples successfully.

The SEM images are shown in Fig. 2. The SEM images of N-AC 600 (Fig. 2a), N-AC 700 (Fig. 2b), and N-AC 800 (Fig. 2c) show the formation of a typical porous carbon structure. The porous surface of N-AC 600, N-AC 700, and N-AC 800 could be seen by the presence of holes on the carbon surface after the KOH activation. The energy-dispersive X-ray spectroscopy (EDS) mapping study of three carbon samples is shown in Fig. 2. A uniform distribution of N on the surface was observed. This result shows that N has been successfully doped into these activated materials. From Fig. 2e to g, we can find that there are obvious quantitative differences among N-AC 600, N-AC 700, and N-AC 800. The N content decreases with the pyrolysis temperature. Form the transmission electron microscopy (TEM) figures (Fig. 3), apparent oriented multilayer domains and a few indistinguishable grapheme sheets stacked in parallel positions were observed in all nitrogen-doped carbon samples. Arranged structure with uniform pores was also clearly observed, implying that nitrogen-doped carbons possess a well ordered 2D hexagonal microstructure with 1D channels. The thermogravimetric analysis (TGA) curves of the three carbon samples are shown in Fig. S3. It needs to be noted that the N-AC samples is stable up to 350 °C in nitrogen; which is significantly more stable than MOFs and POFs [40,41].

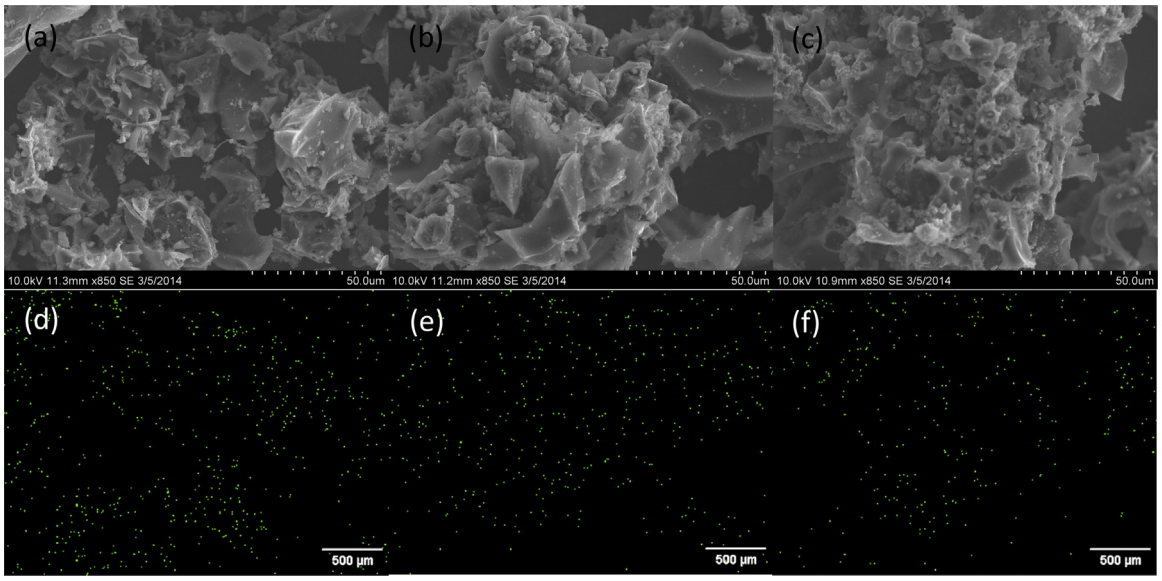

Fig. 2. SEM images of (a) N-AC 600, (b) N-AC 700, (c) N-AC 800, (d) N-AC 600 EDS mapping for N, (e) N-AC 700 EDS mapping for N, (f) N-AC 800 EDS mapping for N.

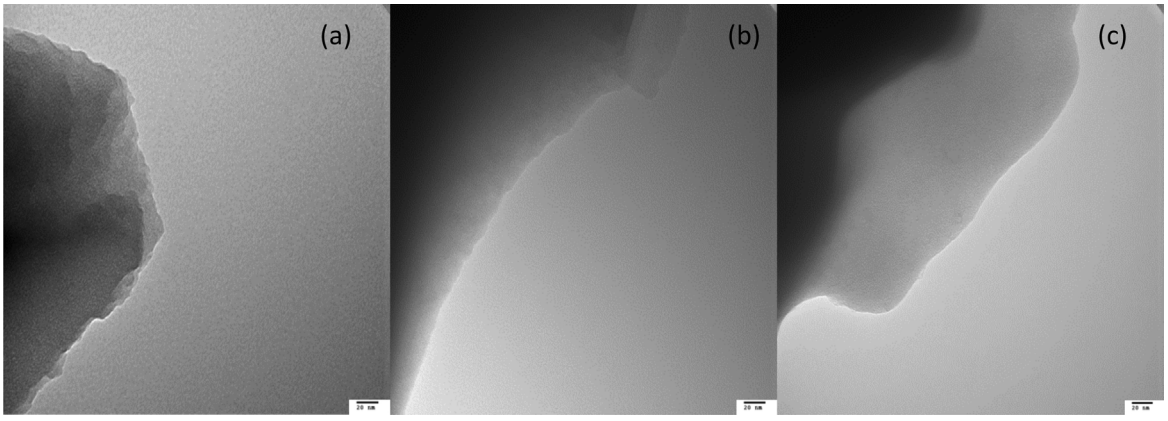

Fig. 3. TEM images of (a) N-AC 600, (b) N-AC 700, and (c) N-AC 800.

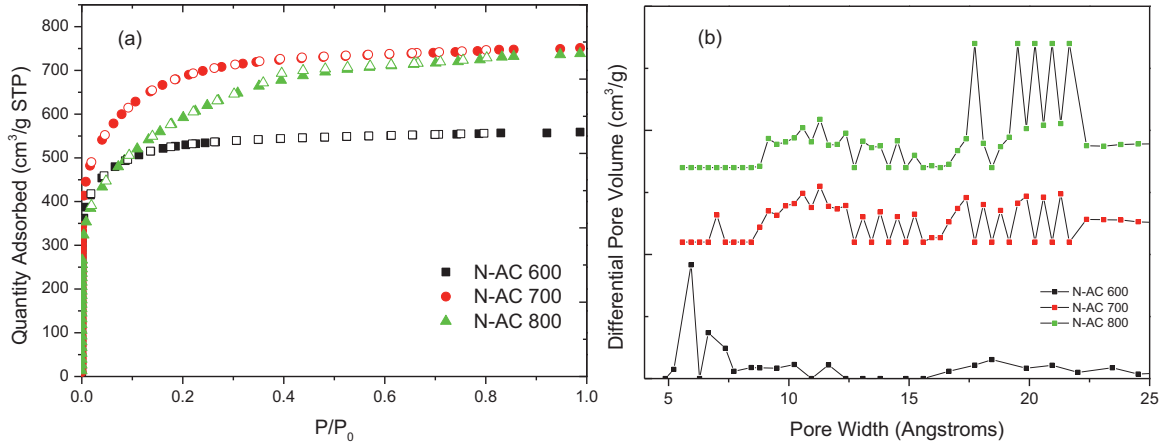

Fig. 4. (a) The N2 adsorption (filled symbol) – desorption (open symbol) isotherms at 77 K and (b) pore size distribution of N-AC 600, N-AC 700, and N-AC 800.

3.2. *Pore sizes and pore volumes*

To determine the pore textural properties of these carbon samples, nitrogen adsorption and desorption isotherms on all three samples at 77 K, as shown in Fig. 4, were measured. The N_2 isotherms of all three samples display a typical type I shape according to IUPAC classification [42]. The steep adsorption at low pressures indicates that the nitrogen-doped carbons have a predominant microporous structure (<2 nm), which is clearly shown in pore size distribution in Fig. 4b. The micropore size distribution and

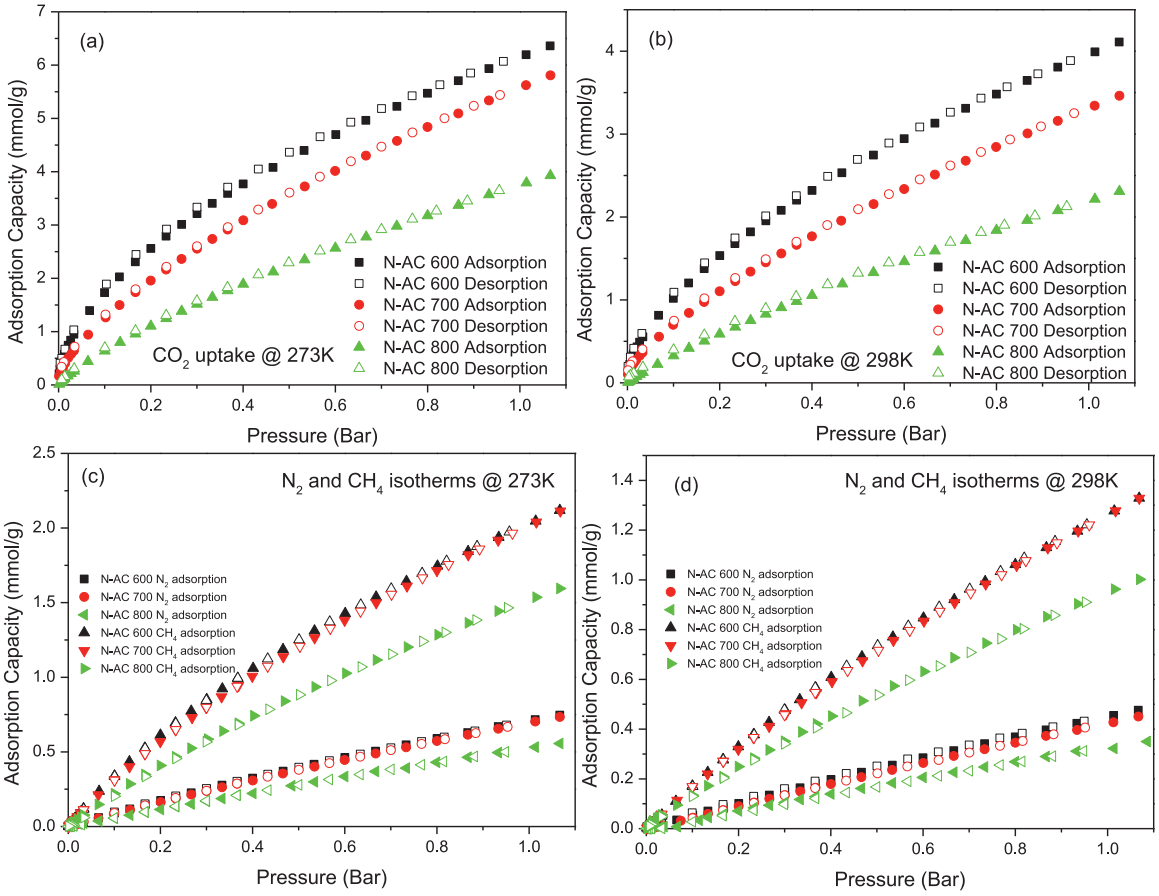

Fig. 5. (a) CO_2 adsorption 273 K and (b) CO_2 adsorption 298 K (c) N_2 and CH_4 adsorption 273 K and (d) N_2 and CH_4 adsorption 298 K of N-AC 600, N-AC 700, and N-AC 800.

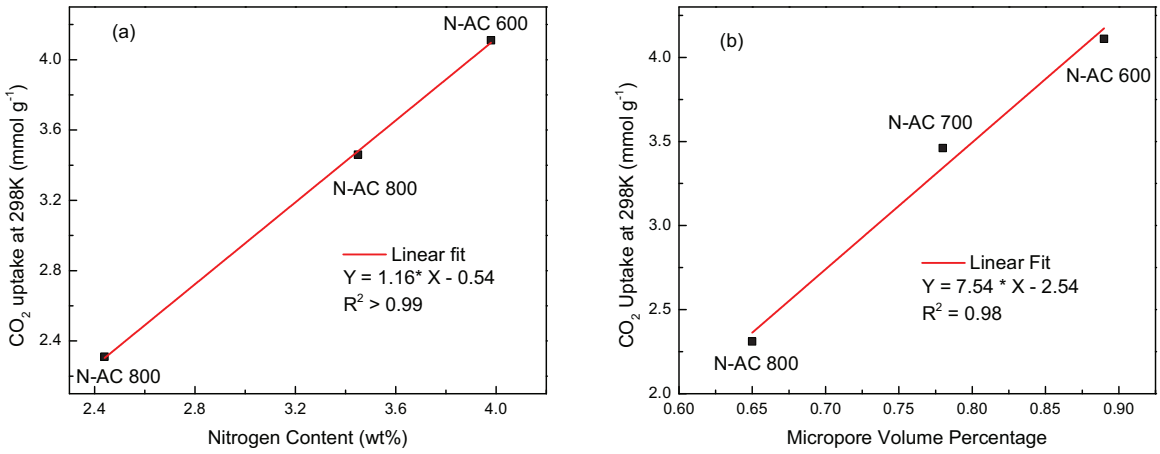

Fig. 6. (a) Nitrogen content correlated with CO_2 uptake at 298 K and (b) micropore volume percentage correlated with CO_2 uptake at 298 K.

pore volume were calculated by the Non-Localized Density Functional Theory (NLDFT) method. The median pore size of N-AC 600 is the smallest among three adsorbents. The median pore size is 0.7, 0.9, and 1.2 nm for N-AC 600, N-AC 700, and N-AC 800, respectively. A lot of efforts have been made to increase CO_2 capacity under 1 atm, for example, increasing BET surface area [43], modifying pore structure [44], and doping functional groups [45,46]. The largest BET surface area we obtained was 2146 $m^2 g^{-1}$ for N-AC 700, and 1629 and 1934 $m^2 g^{-1}$ for N-AC 600 and N-AC 800, respectively. This result is comparable with the reported values for recently investigated ordered mesoporous carbons [7].

3.3. *Adsorption isotherms of CO_2, CH_4, and N_2*

As shown in Fig. 5 and Fig. S4, the adsorption isotherms of CO_2, N_2, and CH_4 were measured at three different temperatures (273, 298, and 323 K) and gas pressures up to 1 bar. All isotherms show excellent reversibility without any hysteresis, indicating that the adsorbed molecules can be easily desorbed under a vacuum in the desorption step. Thus, the nitrogen-doped porous carbon adsorbents can be easily regenerated without any additional thermal energy input, which makes the nitrogen-doped porous carbon adsorbents energy efficient for industrial applications. All

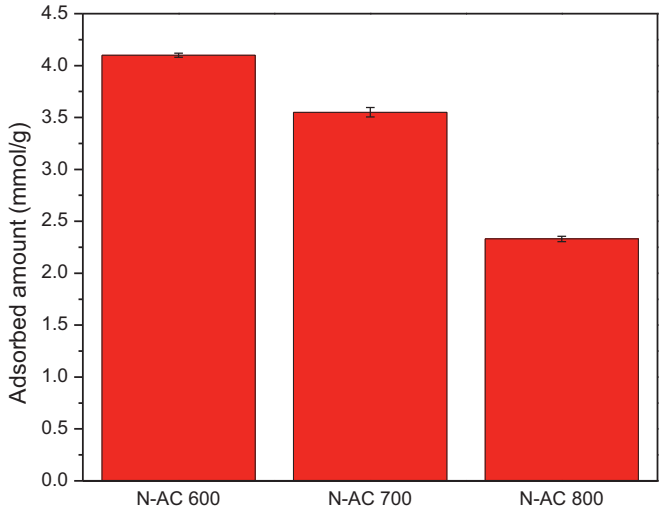

Fig. 7. CO_2 adsorption and cyclic test of CO_2 on three sample at 298 K.

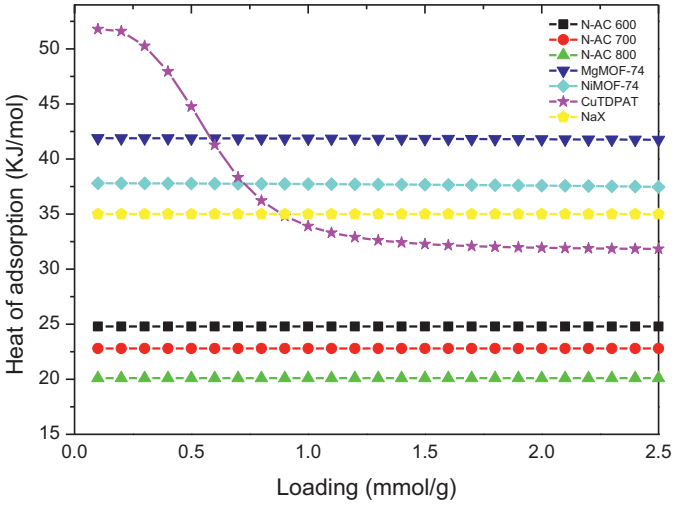

Fig. 8. Isosteric heats of adsorption for CO_2 on the N-ACs, MgMOF-74, NiMOF-74Cu-TDPA, and NaX.

adsorption isotherms were fitted by Langmuir–Freundlich model, the detailed calculations and equation parameters are summarized in Supporting Material (Tables S1–S3). It is clear that the nitrogen-doped porous carbon adsorbents adsorb CO_2 much more than N_2 and CH_4, because of its higher quadrupole moment and polarizability. CH_4 is preferentially adsorbed over N_2 because the polarizability of CH_4 is higher than that of N_2 [47,48]. The highest CO_2 capacity at 100 kPa is obtained by N-AC 600, which is 6.36 and 4.11 mmol g^{-1} at 273 and 298 K, respectively. These values are much higher than other well-known carbon adsorbents rerpoted in the literature, such as sOMC (~2.0 mmol g^{-1}) [7], VR5 (~3.8 mmol g^{-1}) [49], and commercial AC (~0.9 mmol g^{-1}) [50] at 298 K and 100 kPa. They are also comparable with other high quality functionally doped activated carbons, such as S-doped activated carbon (~4.5 mmol g^{-1}) [51] and N-doped activated carbon (~4.3 mmol g^{-1}) [14] at 298 K and 100 kPa. The capacity is also superior to other adsorbents, such as MOFs [52–54], HCPs [55,56] and PAFs [57]. The nitrogen-doped porous carbon adsorbents show a high CH_4 adsorption capacity as well (2.1 and 1.3 mmol g^{-1} on N-AC 600 at 273 and 298 K, respectively, at the100 kPa). These values are higher than the CH_4 adsorption capacity of other adsorbents including zeolite 5A (~0.8 mmol g^{-1}) [58] and ZIF-68 (~0.5 mmol g^{-1}) [59]. In flue gas CO2 capture applications, which

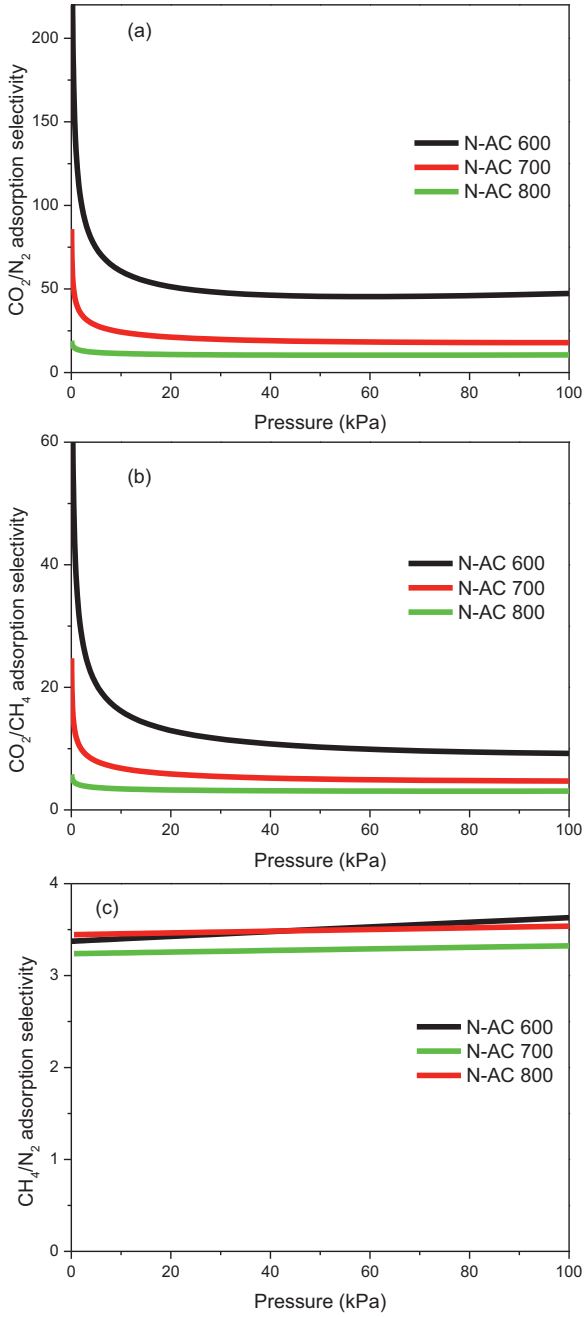

Fig. 9. IAST predicted adsorption selectivities for equimolar binary mixtures of (a)CO_2/CH_4, (b)CH_4/N_2, and (c) CO_2/N_2.

typically contains less than 15% CO2, thus, the adsorption capacity at low pressure (~0.15 bar) is critical to evaluate adsorbents. A very high CO2 uptake (1.35 mmol g^{-1}) is obtained on N-600 at 298 K and 0.15 bar. A lower CO_2 uptake (0.94 mmol g^{-1} and 0.45 mmol g^{-1}) is observed on N-700 and N-800, respectively, under the same condition. Compared with other recently reported adsorbents the result is still outstanding, such as, the S-containing activated carbon (1.3 mmol g^{-1}) [51] and N-containing activated carbon (1.2 mmol g^{-1}) [14].

In order to investigate the factors on CO_2 adsorption, we correlate N-content and microporous volume percentage versus CO_2 uptake shown in Fig. 6. The effect of N-content on CO_2 adsorption equilibrium is shown in Fig. 6a. A good linear correlation ($R^2 > 0.99$) was obtained between CO_2 capacity and N-content, which clearly demonstrate the efficacy of preserving more N-containing group

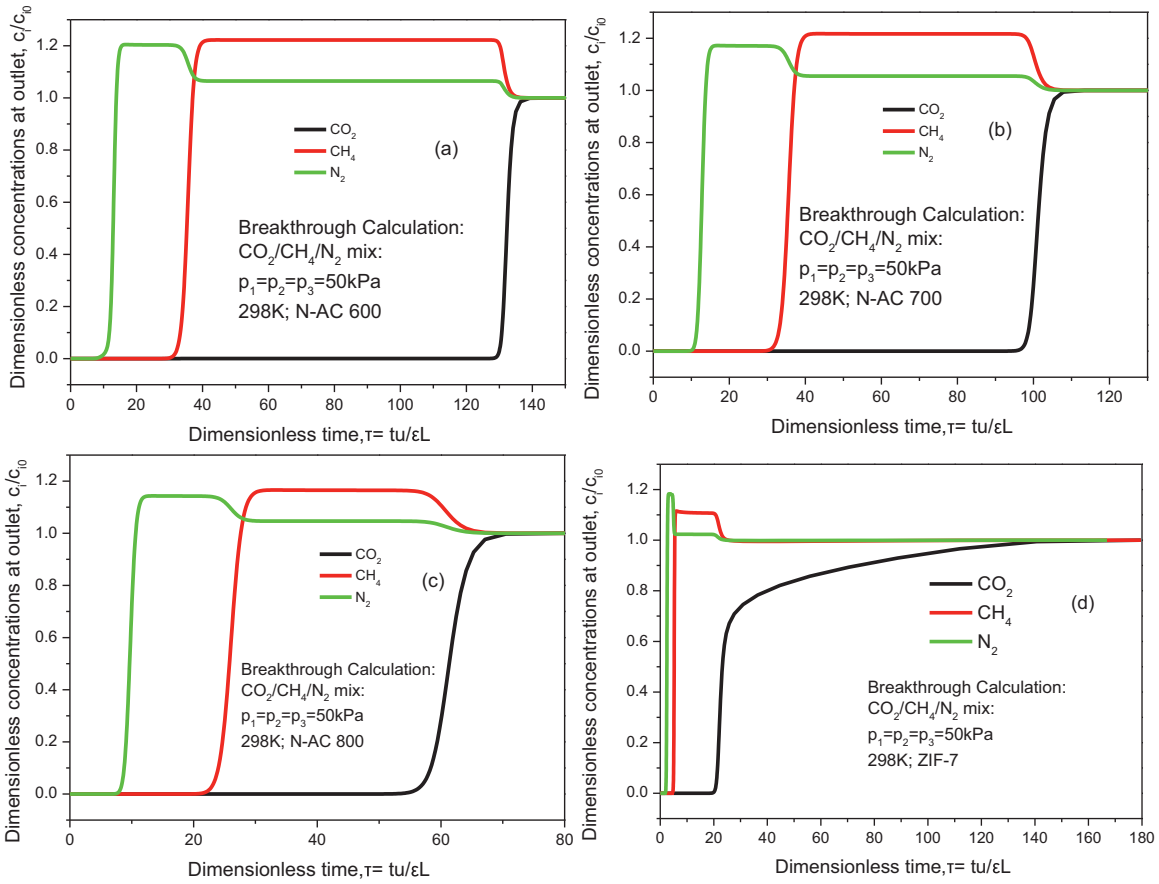

Fig. 10. Breakthrough simulation data of (a)N-AC 600, (b) N-AC 700, (c) N-AC 800, and (d) ZIF-7 at 298 K and 1 bar for an equimolar $CO_2/CH_4/N_2$ mixture, (c_i, the concentration of outlet gas; c_0, the concentration of inlet gas).

on activated samples for enhancing their affinity for adsorbing CO_2. The impact of micropore volume on CO_2 capacity is also explored as shown in Fig. 6b. Excellent linear correlation ($R^2 = 0.98$) was observed, which means micropore volume and CO_2 uptake are strongly associated. It is noteworthy that, actually, micropores are the dominant in determining CO_2 capture ability rather than meso- and macropores. It is reasonable to conclude that N-content and micropore structure are both important to CO_2 capture performances.

In terms of practical applications, the adsorbents are required to give repeatable CO_2 adsorption capacities in multiple regeneration cycles. Thus, we measured extra five CO_2 adsorption cycles at 298 K for all three samples. As shown in Fig. 7, adsorption capacities for five runs are nearly identical for each sample respectively. This suggests that those adsorbents are pretty stable and are able to reuse.

3.4. Isosteric heat of adsorption

Besides the adsorption isotherms, the isosteric heat of adsorption was also commonly used to analyze the interaction relationship. The isosteric heat of adsorption, Q_{st}, defined as

$$Q_{st} = RT^2 \left(\frac{\partial \ln p}{\partial T} \right)_q$$

were determined using the pure component isotherm fits using the Clausius–Clapeyron equation, where Qst (kJ/mol) is the isosteric heat of adsorption, T (K) is the temperature, p (kPa) is the pressure, R is the gas constant. The values of Q_{st} for CO_2, CH_4, and N_2 are provided in Table S4 in each of three carbon samples. Fig. 8 presents a comparison of the isosteric heats of adsorption of CO_2 in N-AC 600, N-AC 700, and N-AC 800 with data from the published literature for NaX zeolite [60], MgMOF-74 [60], Cu-TDPAT [61], and NiMOF-74 [62,63]. Also, the adsorption heat decreases with the carbon activation temperature, indicating that more N-containing group is removed at higher temperatures. This can be confirmed by the EDS mapping images shown in Fig. 2. We note the Q_{st} values of CO_2 in the nitrogen-doped carbons are significantly lower than that of NaX zeolite and also MOFs such as MgMOF-74, NiMOF-74, and Cu-TDPAT. This implies that the cost of regeneration with N-ACs will be significantly lower than that of other materials. This is an important advantage in favor of nitrogen-doped carbons in industrial applications.

3.5. Separation of binary mixtures

The selectivity is a very critical parameter in selecting suitable adsorbents. In all the calculations to be presented below, the calculations of q_1 and q_2 are based on the use of the Ideal Adsorbed Solution Theory (IAST) of Myers and Prausnitz [64]. The accuracy of the IAST calculations for estimation of the component loadings for several binary mixtures in a wide variety of zeolites and MOFs has been established by comparison with Configurational-Bias Monte Carlo (CBMC) simulations of mixture adsorption [65–67]. Further details are provided in Supporting material.

Fig. 9 presents the values of the adsorption selectivity for equimolar binary CO_2/CH_4, CO_2/N_2, and CH_4/N_2 gas mixtures maintained at isothermal conditions at 298 K in N-AC 600, N-AC 700, and N-AC 800. For CO_2/CH_4 and CO_2/N_2 mixtures, the highest adsorption selectivities are obtained with N-AC 600 of 9.2 and

47.3 at 100 kPa, respectively. The CO_2/N_2 selectivity is significantly higher than other adsorbents, such as, ordered mesoporous carbon (~11.33) [7], MIL-47(v) (~9) [68], and N-doped hierarchical carbons (~8.4) [69] at 298 K and 100 kPa, which strongly suggests that the nitrogen-doped carbon adsorbent (N-AC 600) is a better adsorbent for capturing CO_2 from flue gas. N-AC 600 displayed a CO_2/CH_4 selectivity of 9.2 at 298 K and 100 kPa, this value is better than the most existing adsorbents at a similar condition, such as, silicalite-1 (~2.6) [70], SBA-15 (~5.5) [71], and MCM-41 (~5.5) [72]. For CH_4/N_2 gas mixtures, the adsorption selectivities of N-AC 600 and N-AC 700 are nearly the same, and higher than that of N-AC 800. At 298 K and 100 kPa, a CH_4/N_2 selectivity of 3.6 is obtained, which is higher than IRMOF-1 (~2) [73] and ZIF-69 (~3) [68]. Those comparisons indicate the nitrogen-doped carbons are promising adsorbents in flue gas and natural gas processing.

3.6. Transient breakthrough simulations

To demonstrate a potential application of these carbon adsorbents for gas separation, a breakthrough simulation with the nitrogen-doped adsorbents was conducted. Separations using porous adsorbents are usually conducted in the fixed bed units; in such cases the separation performance is dictated by a combination of adsorption selectivity and uptake capacity. For a proper evaluation of the performance of fixed bed adsorbers it is necessary to carry out transient breakthrough simulations as described in the literature [74,75]. We therefore, performed transient breakthrough simulations for separation of $CO_2/CH_4/N_2$ gas mixtures on N-ACs. The methodology details and movies using the adsorption cycle isotherms fits are provided in Supplementary material; the methodology used has been verified to be of good accuracy [74,76]. In this study, the simulation parameters are bed length (L = 1.8 m), voidage of bed (ϵ = 0.5), superficial gas velocity (u = 0.05 m/s), and interstitial velocity (v = 0.1 m/s). Fig. 10 compares $CO_2/CH_4/N_2$ mixture breakthrough characteristics as a function of the dimensionless time, $\tau = \frac{tu}{L\epsilon}$. For all three N-ACs the sequence of breakthroughs is N_2, CH_4, and CO_2, this is dictated by the hierarchy of adsorption strengths. CO_2 molecules are strongly adsorbed by N-ACs, which elutes last in the sequence. The longest retention time obtained on N-AC 600 and this material has the best separation performance due to its highest CO_2 capacity and highest CO_2/N_2 and CO_2/CH_4 adsorption selectivities. We noted that there is a time interval that we can get pure CH_4 or N_2 using N-ACs. We compare N-ACs with ZIF-7 using breakthrough simulation under the same condition. The CO_2 and CH_4 adsorption data of ZIF-7 are from one recently published paper by our group [77], the N_2 adsorption is obtained from US Patent [78]. The simulation curves are summarized in Fig. 10. According to Fig. 10d, the retention time of CO_2 on ZIF-7 is much shorter than N-ACs. This indicates the time interval to separate CO_2/CH_4 and CO_2/N_2 is shorter than N-ACs. The CH_4/N_2 separation time is even shorter, we almost can't separate them efficiently. As a result, the nitrogen-doped porous carbons have a higher equilibrium separation ability of $CO_2/CH_4/N_2$ than ZIF-7.

4. Conclusion

Three highly porous nitrogen-doped carbon adsorbents have been synthesized successfully with KOH as the porogen agent at 600, 700, and 800 °C, respectively. The largest BET specific surface area of these carbons is 2146 $m^2\,g^{-1}$ obtained on N-AC 700. Overall, the best adsorbent among these three carbons is N-AC 600 that has the highest CO_2 adsorption capacity of 6.36 and 4.11 mmol g^{-1} at 100 kPa and 273 and 298 K, respectively. Moreover, CO_2/N_2 adsorption selectivity N-AC 600 is much larger than other adsorbents for CO_2 capture in flue gas. Potential applications of these carbon adsorbents for CO_2 capture in flue gas and natural gas upgrading is demonstrated by adsorption breakthrough simulation calculations. The high CO_2 adsorption capacity, large separation selectivity and low isosteric heats of adsorption make these nitrogen-doped adsorbents very promising for CO_2 capture in flue gas and natural gas upgrade.

Supporting materials

A supporting document presenting additional experimental data and simulation method, and a movie showing the simulated gas concentration profiles inside a column packed with N-AC 600 during an adsorption breakthrough run are uploaded.

Acknowledgments

This project was partially supported by U.S. National Aeronautics and Space Administration (New Mexico Space Grant), U.S. National Science Foundation (EEC 1028968), New Mexico State University Office of Vice President for Research (GREG awards for J. Wang). J. Yang acknowledges Taiyuan University of Technology for supporting his visit to New Mexico State University. Kodanda Phani Raj Dandamudi acknowledges Assistant Professor F. Omar Holgui in Plant and Environment Sciences Department at New Mexico State University for the element analyzer.

Appendix A. Supplementary data

Supplementary data associated with this article can be found, in the online version, at http://dx.doi.org/10.1016/j.mtcomm.2015.06.009

References

[1] D. Aaron, C. Tsouris, Separation of CO_2 from flue gas: a review, Sep. Sci. Technol. 40 (1–3) (2005) 321–348.
[2] E.S. Kikkinides, R.T. Yang, S.H. Cho, Concentration and recovery of Co_2 from flue-gas by pressure swing adsorption, Ind. Eng. Chem. Res. 32 (11) (1993) 2714–2720.
[3] S. Hermansson, F. Lind, H. Thunman, On-line monitoring of fuel moisture-content in biomass-fired furnaces by measuring relative humidity of the flue gases, Chem. Eng. Res. Des. 89 (11A) (2011) 2470–2476.
[4] P. Mohanty, L.D. Kull, K. Landskron, Porous covalent electron-rich organonitridic frameworks as highly selective sorbents for methane and carbon dioxide, Nat. Commun. (2011) 2.
[5] R.W. Baker, K. Lokhandwala, Natural gas processing with membranes: an overview, Ind. Eng. Chem. Res. 47 (7) (2008) 2109–2121.
[6] R.H. Hugman, E.H. Vidas, P.S. Springer, Chemical composition of discovered and undiscovered natural gas in the lower-48 United States, in: Project Summary Final report, 1 November 1988–31 March, 1990.
[7] B. Yuan, X.F. Wu, Y.X. Chen, J.H. Huang, H.M. Luo, S.G. Deng, Adsorption of CO_2, CH_4, and N-2 on ordered mesoporous carbon: approach for greenhouse gases capture and biogas upgrading, Environ. Sci. Technol. 47 (10) (2013) 5474–5480.
[8] X. Zhong, F. Yao, X. Low, Z. Chen, M. He, H.T. Wang, Carbon composite membrane derived from a two-dimensional zeolitic imidazolate framework and its gas separation properties, Carbon 72 (2014) 242–249.
[9] R. Krishnamurthy, M.J. Andrecovich, Removal of particulate matter and trace contaminatnts, separation, liquifying carbon dioxide, distillation. Google Patents: 1993.
[10] G.T. Rochelle, Amine scrubbing for CO_2 capture, Science 325 (5948) (2009) 1652–1654.
[11] A.R. Kulkarni, D.S. Sholl, Analysis of equilibrium-based TSA processes for direct capture of CO_2 from air, Ind. Eng. Chem. Res. 51 (25) (2012) 8631–8645.
[12] S.Y. Lee, S.J. Park, Isothermal exfoliation of graphene oxide by a new carbon dioxide pressure swing method, Carbon 68 (2014) 112–117.
[13] D.Y. Kim, H.M. Lee, S.K. Min, Y. Cho, I.C. Hwang, K. Han, J.Y. Kim, K.S. Kim, CO_2 capturing mechanism in aqueous ammonia: NH3-driven decomposition-recombination pathway, J. Phys. Chem. Lett. 2 (7) (2011) 689–694.
[14] V. Chandra, U. Yu, H. Kim, S. Yoon, Y. Kim, H. Kwon, M. Meyyappan, K.S. Kim, Highly selective CO_2 capture on N-doped carbon produced by chemical activation of polypyrrole functionalized graphene sheets, Chem. Commun. 48 (5) (2012) 735–737.

[15] V.S.P.K. Neti, J. Wang, S.G. Deng, L. Echegoyen, Selective CO_2 adsorption in a porphyrin polymer with benzimidazole linkages, Rsc. Adv. 5 (15) (2015) 10960–10961.
[16] C. Petit, T.J. Bandosz, Enhanced adsorption of ammonia on metal-organic framework/graphite oxide composites: analysis of surface interactions, Adv. Funct. Mater. 20 (1) (2010) 111–118.
[17] X.F. Wu, Z.B. Bao, B. Yuan, J. Wang, Y.Q. Sun, H.M. Luo, S.G. Deng, Microwave synthesis and characterization of MOF-74 (M = Ni, Mg) for gas separation, Micropor. Mesopor. Mater. 180 (2013) 114–122.
[18] J. Wang, J.H. Huang, X.F. Wu, B. Yuan, Y.Q. Sun, Z.L. Zeng, S.G. Deng, Effect of nitrogen group on selective separation of CO_2/N-2 in porous polystyrene, Chem. Eng. J. 256 (2014) 390–397.
[19] C.D. Wood, B. Tan, A. Trewin, F. Su, M.J. Rosseinsky, D. Bradshaw, Y. Sun, L. Zhou, A.I. Cooper, Microporous organic polymers for methane storage, Adv. Mater. 20 (10) (2008) 1916–1921.
[20] A.I. Cooper, Conjugated microporous polymers, Adv. Mater. 21 (12) (2009) 1291–1295.
[21] J.X. Jiang, F. Su, A. Trewin, C.D. Wood, H. Niu, J.T.A. Jones, Y.Z. Khimyak, A.I. Cooper, Synthetic control of the pore dimension and surface area in conjugated microporous polymer and copolymer networks, J. Am. Chem. Soc. 130 (24) (2008) 7710–7720.
[22] R. Serna-Guerrero, E. Da'na, A. Sayari, New insights into the interactions of CO(2) with amine-functionalized silica, Ind. Eng. Chem. Res. 47 (23) (2008) 9406–9412.
[23] F.H. Bai, Y.D. Xia, B.L. Chen, H.Q. Su, Y.Q. Zhu, Preparation and carbon dioxide uptake capacity of N-doped porous carbon materials derived from direct carbonization of zeolitic imidazolate framework, Carbon 79 (2014) 213–226.
[24] L. Bastin, S. Barcia, J. Hurtado, C. Silva, E. Rodrigues, B.L. Chen, A microporous metal-organic framework for separation of CO_2/N-2 and CO_2/CH4 by fixed-bed adsorption, J. Phys. Chem. C 112 (5) (2008) 1575–1581.
[25] Y. Luo, B. Li, W. Wang, K. Wu, B. Tan, Hypercrosslinked aromatic heterocyclic microporous polymers: a new class of highly selective CO_2 capturing materials, Adv. Mater. 24 (42) (2012) 5703–5707.
[26] S.-H. Liu, C.-H. Wu, H.-K. Lee, S.-B. Liu, Highly stable amine-modified mesoporous silica materials for efficient CO_2 capture, Top. Catal. 53 (3–4) (2010) 210–217.
[27] H. Seema, C. Kemp, H. Le, S.-W. Park, V. Chandra, W. Lee, K.S. Kim, Highly selective CO_2 capture by S-doped microporous carbon materials, Carbon 66 (0) (2014) 320–326.
[28] D. Qian, Lei C, E.-M. Wang, W.-C. Li, A.-H. Lu, A method for creating microporous carbon materials with excellent CO_2-adsorption capacity and celectivity, ChemSusChem 7 (1) (2014) 291–298.
[29] H. Wei, S. Deng, B. Hu, Z. Chen, B. Wang, J. Huang, G. Yu, Granular bamboo-derived activated carbon for high CO(2) adsorption: the dominant role of narrow micropores, ChemSusChem 5 (12) (2012) 2354–2360.
[30] M. Nandi, K. Okada, A. Dutta, A. Bhaumik, J. Maruyama, D. Derks, H. Uyama, Unprecedented CO_2 uptake over highly porous N-doped activated carbon monoliths prepared by physical activation, Chem. Commun. 48 (83) (2012) 10283–10285.
[31] Aijaz Arshad, Naoko Fujiwara, Qiang Xu, From metal-organic framework to nitrogen-decorated nanoporous carbons: high CO_2 uptake and efficient catalytic oxygen reduction, J. Am. Chem. Soc. 136 (19) (2014) 6790–6793.
[32] X. Fan, L. Zhang, G. Zhang, Z. Shu, J. Shi, Chitosan derived nitrogen-doped microporous carbons for high performance CO_2 capture, Carbon 61 (2013) 423–430.
[33] V. Chandra, S.U. Yu, S.H. Kim, Y.S. Yoon, D.Y. Kim, A.H. Kwon, M. Meyyappan, K.S. Kim, Highly selective CO_2 capture on N-doped carbon produced by chemical activation of polypyrrole functionalized graphene sheets, Chem. Commun. (Cambridge, England) 48 (5) (2012) 735–737.
[34] J. Yu, M. Guo, F. Muhammad, A. Wang, G. Yu, H. Ma, G. Zhu, Simple fabrication of an ordered nitrogen-doped mesoporous carbon with resorcinol–melamine–formaldehyde resin, Micropor. Mesopor. Mater. 190 (2014) 117–127.
[35] C. Chen, J. Kim, W.-S. Ahn, Efficient carbon dioxide capture over a nitrogen-rich carbon having a hierarchical micro-mesopore structure, Fuel 95 (2012) 360–364.
[36] F.B. Su, C.K. Poh, J.S. Chen, G.W. Xu, D. Wang, Q. Li, J.Y. Lin, X.W. Lou, Nitrogen-containing microporous carbon nanospheres with improved capacitive properties, Energy Environ. Sci. 4 (3) (2011) 717–724.
[37] Y.W. Zhu, S. Murali, M.D. Stoller, K.J. Ganesh, W.W. Cai, P.J. Ferreira, A. Pirkle, R.M. Wallace, K.A. Cychosz, M. Thommes, D. Su, E.A. Stach, R.S. Ruoff, Carbon-based supercapacitors produced by activation of graphene, Science 332 (6037) (2011) 1537–1541.
[38] A.C. Ferrari, J. Robertson, Interpretation of Raman spectra of disordered and amorphous carbon, Phys. Rev. B 61 (20) (2000) 14095–14107.
[39] L.G. Cancado, et al., Influence of the atomic structure on the Raman spectra of graphite edges, Phys. Rev. Lett. 93 (24) (2004) 247401.
[40] Z.H. Xiang, X. Peng, X. Cheng, X.J. Li, D.P. Cao, CNT@Cu-3(BTC)(2) and metal-organic frameworks for separation of CO_2/CH_4 mixture, J. Phys. Chem. C 115 (40) (2011) 19864–19871.
[41] A.P. Katsoulidis, M.G. Kanatzidis, Mesoporous hydrophobic polymeric organic frameworks with bound surfactants. Selective adsorption of C_2H_6 versus CH4, Chem. Mater. 24 (3) (2012) 471–479.
[42] K.S.W. Sing, D.H. Everett, R.A.W. Haul, L. Moscou, R.A. Pierotti, J. Rouquerol, T. Siemieniewska, Reporting physisorption data for gas solid systems with special reference to the determination of surface-area and porosity (Recommendations 1984), Pure Appl. Chem. 57 (4) (1985) 603–619.
[43] T. Ben, Y. Li, L. Zhu, D. Zhang, D. Cao, Z. Xiang, X. Yao, S. Qiu, Selective adsorption of carbon dioxide by carbonized porous aromatic framework (PAF), Energy Environ. Sci. 5 (8) (2012) 8370–8376.
[44] W.G. Lu, D.Q. Yuan, J.L. Sculley, D. Zhao, R. Krishna, H.C. Zhou, Sulfonate-grafted porous polymer networks for preferential CO_2 adsorption at low pressure, J. Am. Chem. Soc. 133 (45) (2011) 18126–18129.
[45] J.X. Song, T. Xu, M.L. Gordin, P.Y. Zhu, D.P. Lv, Y.B. Jiang, Y.S. Chen, Y.H. Duan, D.H. Wang, Nitrogen- doped mesoporous carbon promoted chemical adsorption of sulfur and fabrication of high- areal- capacity sulfur cathode with exceptional cycling stability for lithium- sulfur batteries, Adv. Funct. Mater. 24 (9) (2014) 1243–1250.
[46] P.Z. Li, Y.L. Zhao, Nitrogen-rich porous adsorbents for CO_2 capture and storage, Chem.-Asian J. 8 (8) (2013) 1680–1691.
[47] Y.S. Bae, O.K. Farha, J.T. Hupp, R.Q. Snurr, Enhancement of CO_2/N-2 selectivity in a metal-organic framework by cavity modification, J. Mater. Chem. 19 (15) (2009) 2131–2134.
[48] P.J.E. Harlick, F.H. Tenzel, Adsorption of carbon dioxide, methane and nitrogen: pure and binary mixture adsorption for ZSM-5 with SiO_2/Al_2O_3 ratio of 280, Sep. Purif. Technol. 33 (2) (2003) 199–210.
[49] M.E. Casco, M. Martinez-Escandell, J. Silvestre-Albero, F. Rodriguez-Reinoso, Effect of the porous structure in carbon materials for CO_2 capture at atmospheric and high-pressure, Carbon 67 (2014) 230–235.
[50] X.Y. Ma, M.H. Cao, C.W. Hu, Bifunctional HNO_3 catalytic synthesis of N-doped porous carbons for CO_2 capture, J. Mater. Chem. A 1 (3) (2013) 913–918.
[51] H. Seema, K.C. Kemp, N.H. Le, S.W. Park, V. Chandra, J.W. Lee, K.S. Kim, Highly selective CO_2 capture by S-doped microporous carbon materials, Carbon 66 (2014) 320–326.
[52] J. An, S.J. Geib, N.L. Rosi, High and selective CO_2 uptake in a cobalt adeninate metal-organic framework exhibiting pyrimidine- and amino-decorated pores, J. Am. Chem. Soc. 132 (1) (2010) 38–39.
[53] R. Banerjee, H. Furukawa, D. Britt, C. Knobler, M. O'Keeffe, O.M. Yaghi, Control of pore size and functionality in isoreticular zeolitic imidazolate frameworks and their carbon dioxide selective capture properties, J. Am. Chem. Soc. 131 (11) (2009) 3875–3877.
[54] M.O. Schach, R. Schneider, H. Schramm, J.U. Repke, Techno-economic analysis of postcombustion processes for the capture of carbon dioxide from power plant flue Gas, Ind. Eng. Chem. Res. 49 (5) (2010) 2363–2370.
[55] B.Y. Li, R.N. Gong, W. Wang, X. Huang, W. Zhang, H.M. Li, C.X. Hu, B.E. Tan, A new strategy to microporous polymers: knitting rigid aromatic building blocks by external cross-linker, Macromolecules 44 (8) (2011) 2410–2414.
[56] M.G. Rabbani, H.M. El-Kaderi, Template-free synthesis of a highly porous benzimidazole-linked polymer for CO_2 capture and H-2 storage, Chem. Mater. 23 (7) (2011) 1650–1653.
[57] D. Saha, S.G. Deng, Adsorption equilibria and kinetics of carbon monoxide on zeolite 5A, 13X MOF-5, and MOF-177, J. Chem. Eng. Data 54 (8) (2009) 2245–2250.
[58] N.K. Jensen, T.E. Rufford, G. Watson, D.K. Zhang, K.I. Chan, E.F. May, Screening zeolites for gas separation applications involving methane, nitrogen, and carbon dioxide, J. Chem. Eng. Data 57 (1) (2012) 106–113.
[59] B. Liu, B. Smit, Molecular simulation studies of separation of CO_2/N-2, CO_2/CH_4, and CH4/N-2 by ZIFs, J. Phys. Chem. C 114 (18) (2010) 8515–8522.
[60] J.A. Mason, K. Sumida, Z.R. Herm, R. Krishna, J.R. Long, Evaluating metal-organic frameworks for post-combustion carbon dioxide capture via temperature swing adsorption, Energy Environ. Sci. 4 (8) (2011) 3030–3040.
[61] H.H. Wu, K.X. Yao, Y.H. Zhu, B.Y. Li, Z. Shi, R. Krishna, J. Li, Cu-TDPAT an rht-type dual-functional metal-organic framework offering significant potential for use in H-2 and natural gas purification processes operating at high pressures, J. Phys. Chem. C 116 (31) (2012) 16609–16618.
[62] R. Krishna, J.M. van Baten, Investigating the relative influences of molecular dimensions and binding energies on diffusivities of guest species inside nanoporous crystalline materials, J. Phys. Chem. C 116 (44) (2012) 23556–23568.
[63] R. Krishna, J.M. van Baten, Investigating the influence of diffusional coupling on mixture permeation across porous membranes, J. Membr. Sci. 430 (2013) 113–128.
[64] A.L. Myers, J.M. Prausnitz, Thermodynamics of mixed-gas adsorption, Aiche J. 11 (1) (1965) 121–127.
[65] R. Krishna, J.M. van Baten, Using molecular simulations for screening of zeolites for separation Of CO_2/CH_4 mixtures, Chem. Eng. J 133 (1–3) (2007) 121–131.
[66] R. Krishna, J.M. van Baten, In silico screening of zeolite membranes for CO_2 capture, J Membr. Sci. 360 (1–2) (2010) 323–333.
[67] R. Krishna, J.M. van Baten, In silico screening of metal-organic frameworks in separation applications, Phys. Chem. Chem. Phys. 13 (22) (2011) 10593–10616.
[68] B. Liu, B. Smit, Comparative molecular simulation study of CO_2/N-2 and CH_4/N-2 separation in zeolites and metal-organic frameworks, Langmuir 25 (10) (2009) 5918–5926.
[69] M.C. Gutierrez, D. Carriazo, C.O. Ania, J.B. Parra, M.L. Ferrer, F. del Monte, Deep eutectic solvents as both precursors and structure directing agents in the synthesis of nitrogen doped hierarchical carbons highly suitable for CO_2 capture, Energy Environ. Sci. 4 (9) (2011) 3535–3544.

[70] J.F. Yang, J.M. Li, W. Wang, L.B. Li, J.P. Li, Adsorption of CO_2, CH_4, and N-2 on 8-10-, and 12-membered ring hydrophobic microporous high-silica zeolites: DDR, silicalite-1, and beta, Ind. Eng. Chem. Res. 52 (50) (2013) 17856–17864.
[71] V.K. Saini, M. Andrade, M.L. Pinto, A.P. Carvalho, J. Pires, How the adsorption properties get changed when going from SBA-15 to its CMK-3 carbon replica, Sep. Purif. Technol. 75 (3) (2010) 366–376.
[72] Y. Belmabkhout, R. Serna-Guerrero, A. Sayari, Adsorption of CO_2 from dry gases on MCM-41 silica at ambient temperature and high pressure. 1: pure CO_2 adsorption, Chem. Eng. Sci. 64 (17) (2009) 3721–3728.
[73] J. Pires, V.K. Saini, M.L. Pinto, Studies on selective adsorption of biogas components on pillared clays: approach for biogas improvement, Environ. Sci. Technol. 42 (23) (2008) 8727–8732.
[74] R. Krishna, J.R. Long, Screening metal-organic frameworks by analysis of transient breakthrough of gas mixtures in a fixed bed adsorber, J. Phys. Chem. C 115 (26) (2011) 12941–12950.
[75] R. Krishna, The Maxwell-Stefan description of mixture diffusion in nanoporous crystalline materials, Micropor. Mesopor. Mater. 185 (2014) 30–50.
[76] Y.B. He, R. Krishna, B.L. Chen, Metal-organic frameworks with potential for energy-efficient adsorptive separation of light hydrocarbons, Energy Environ. Sci. 5 (10) (2012) 9107–9120.
[77] X.F. Wu, M.N. Shahrak, B. Yuan, S.G. Deng, Synthesis and characterization of zeolitic imidazolate framework ZIF-7 for CO_2 and CH_4 separation, Micropor. Mesopor. Mater. 190 (2014) 189–196.
[78] S.C. Reyes, Z. Ni, C.S. Paur, P. Kortunov, J. Zengel, H.W. Deckman, Separation of carbon dioxide from nitrogen utilizing zeolitic imidazolate framework materials. Google Patents: 2012.

Supporting Material

Nitrogen-doped Porous Carbons for Highly Selective CO_2 Capture from Flue Gases and Natural Gas Upgrading

Jun Wang [a], Rajamani Krishna [b], Jiangfeng Yang [c], Shugaung Deng [a*]

[a.] Chemical & Materials Engineering Department

New Mexico State University

Las Cruces, New Mexico, 88003, USA

[b.] van't Hoff Institute for Molecular Sciences

University of Amsterdam

Science Park 904, 1098 XH Amsterdam, The Netherlands

[c.] Research Institute of Special Chemicals

Taiyuan University of Technology

Taiyuan 030024, Shanxi, P.R. China

*Corresponding author: Tel: +1-575-646-4346; Fax: +1-575-646-7706.

E-mail address: sdeng@nmsu.edu

Table of Contents

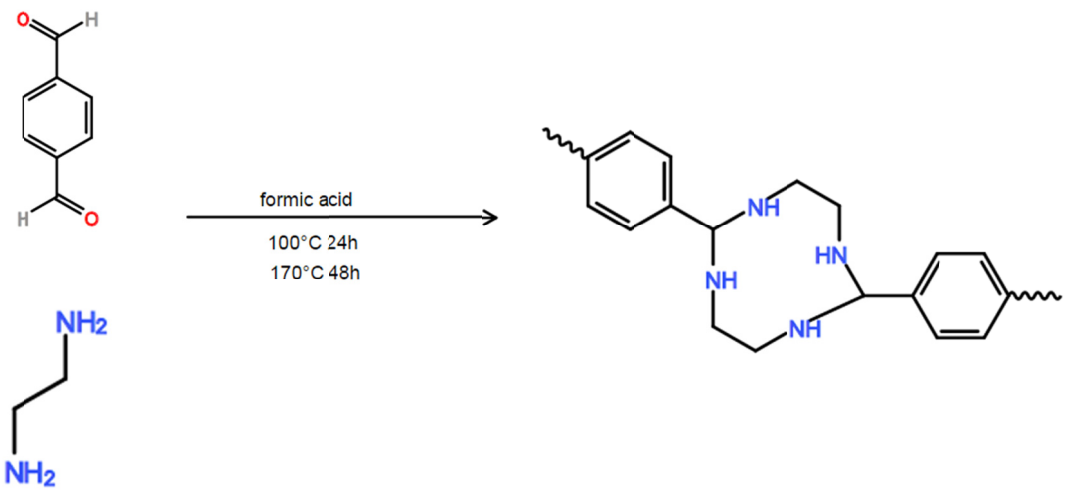

Figure S1. Schematic representation of the N-containing network structure.

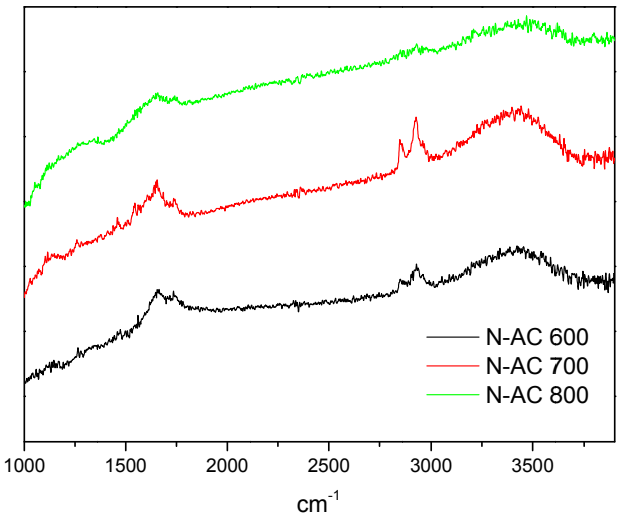

Figure S2. FT-IR spectra of N-ACs.

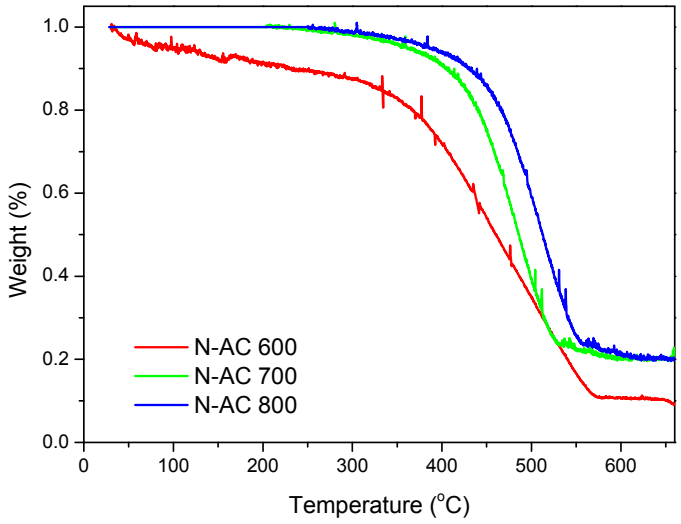

Figure S3. Thermogravimetric analysis of N-ACs.

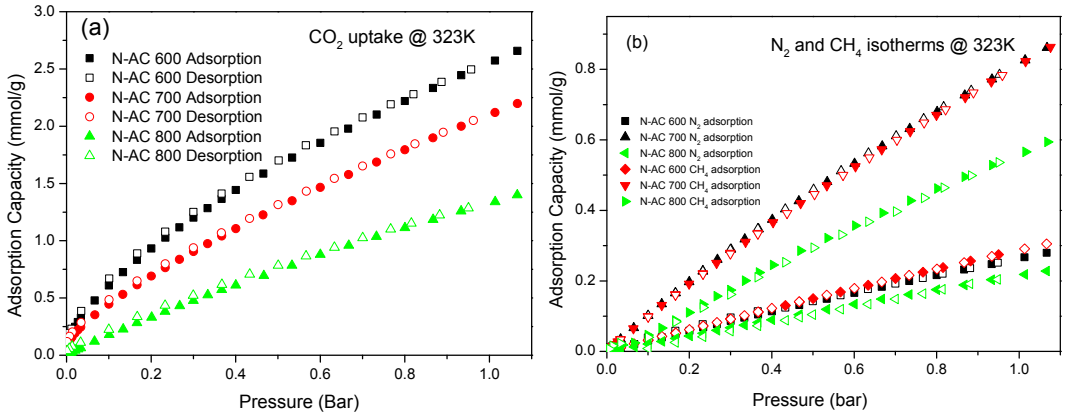

Figure S4. (a) CO_2 adsorption and desorption isotherm 323K and 100 kPa and (b) N_2 and CH_4 adsorption and desorption isotherms 323K and 100 kPa of N-AC 600, N-AC 700, and N-AC 800.

Fitting of pure component isotherms

The experimentally measured loadings for (a) CO_2, (b) CH_4, and (c) N_2 were measured as a function of the absolute pressure at three different temperatures 273 K, 298 K, and 323 K.

The isotherm data for CO_2 were fitted with the Langmuir-Freundlich model

$$q = q_{sat} \frac{bp^{\nu}}{1 + bp^{\nu}} \tag{1}$$

with T-dependent parameter b

$$b = b_0 \exp\left(\frac{E}{RT}\right) \tag{2}$$

The Langmuir-Freundlich parameters for adsorption of CO_2 are provided in Table 1 for N-AC 600, N-AC 700, and N-AC 800.

The simpler single-site Langmuir model

$$q = q_{sat} \frac{bp}{1 + bp}; \quad b = b_0 \exp\left(\frac{E}{RT}\right) \tag{3}$$

was adequate for fitting the isotherm data for CH_4 and N_2; Table 2 and Table 3 provides the T-dependent Langmuir parameters for N-AC 600, N-AC 700, and N-AC 800 for CH_4 and N_2, respectively

	q_{sat} mol kg^{-1}	b_0 Pa$^{-\nu}$	E kJ mol^{-1}	ν dimensionless
N-AC 600	25	4.49×10^{-7}	14.9	0.6
N-AC 700	21.4	3.29×10^{-8}	17.1	0.75
N-AC 800	13.3	4.22×10^{-9}	18.1	0.9

Table S5. Langmuir-Freundlich parameters for adsorption of CO_2 in different AC.

	q_{sat} mol kg^{-1}	b_0 Pa^{-1}	E kJ mol^{-1}
N-AC 600	4.9	2.28×10^{-9}	18.2
N-AC 700	5.4	2.73×10^{-9}	17.4
N-AC 800	4.9	1.84×10^{-9}	17.7

Table S6. 1-site Langmuir parameters for CH_4 in different AC.

	q_{sat} mol kg^{-1}	b_0 Pa^{-1}	E kJ mol^{-1}
N-AC 600	2.9	2.58×10^{-9}	16.2
N-AC 700	4.2	2.91×10^{-9}	14.8
N-AC 800	3.6	2.3×10^{-9}	15

Table S7. 1-site Langmuir parameters for N_2 in different AC.

	Q_{st}, CO_2 kJ mol^{-1}	Q_{st}, CH_4 kJ mol^{-1}	Q_{st}, N_2 kJ mol^{-1}
N-AC 600	24.8	18.2	16.2
N-AC 700	22.8	17.4	14.8
N-AC 800	20.1	17.7	15

Table S8. Isosteric heats of adsorption of CO_2, CH_4 and N_2 in different AC.

IAST calculations

The adsorption selectivity for the mixtures CH_4/N_2 and CO_2/CH_4 defined by

$$S_{ads} = \frac{q_1/q_2}{p_1/p_2}$$

were calculated according to IAST model proposed by Myers [1,2,3]. In above equation, q_1 and q_2 are the absolute component loadings of the adsorbed phase in the mixture. These component loadings are also termed the uptake capacities.

Simulation methodology for transient breakthrough in fixed bed adsorbers

The separation of CO_2/CH_4, CO_2/N_2, and CH_4/N_2 mixtures is commonly carried out in fixed bed adsorbers in which the separation performance is dictated by a combination of three separate factors: (a) adsorption selectivity, (b) uptake capacity, and (c) intra-crystalline diffusivities of guest molecules within the pores. Transient breakthrough simulations are required for a proper evaluation of microporous materials; the simulation methodology used in our work is described in earlier publications [4,5]. A brief summary of the simulation methodology is presented below.

Assuming plug flow of an *n*-component gas mixture through a fixed bed maintained under isothermal conditions (see schematic in Figure **Error! Reference source not found.**), the partial pressures in the gas phase at any position and instant of time are obtained by solving the following set of partial differential equations for each of the species *i* in the gas mixture [6].

$$\frac{1}{RT}\frac{\partial p_i(t,z)}{\partial t} = -\frac{1}{RT}\frac{\partial\left(v(t,z)p_i(t,z)\right)}{\partial z} - \frac{(1-\varepsilon)}{\varepsilon}\rho\frac{\partial \bar{q}_i(t,z)}{\partial t}; \quad i = 1,2,...n \tag{1}$$

In equation (1), t is the time, z is the distance along the adsorber, ρ is the framework density, ε is the bed voidage, v is the interstitial gas velocity, and $\bar{q}_i(t,z)$ is the *spatially averaged* molar loading within the crystallites of radius r_c, monitored at position z, and at time t.

At any time t, during the transient approach to thermodynamic equilibrium, the spatially averaged molar loading within the crystallite r_c is obtained by integration of the radial loading profile

$$\bar{q}_i(t) = \frac{3}{r_c^3}\int_0^{r_c} q_i(r,t) r^2 dr \tag{2}$$

For transient unary uptake within a crystal at any position and time with the fixed bed, the radial distribution of molar loadings, q_i, within a spherical crystallite, of radius r_c, is obtained from a solution of a set of differential equations describing the uptake

$$\frac{\partial q_i(r,t)}{\partial t} = -\frac{1}{\rho}\frac{1}{r^2}\frac{\partial}{\partial r}\left(r^2 N_i\right) \tag{3}$$

The molar flux N_i of component i is described by the simplified version of the Maxwell-Stefan equations in which both correlation effects and thermodynamic coupling effects are considered to be of negligible importance [5]

$$N_i = -\rho D_i \frac{\partial q_i}{\partial r} \tag{4}$$

Summing equation (2) over all n species in the mixture allows calculation of the *total average* molar loading of the mixture within the crystallite

$$\bar{q}_t(t,z) = \sum_{i=1}^{n} \bar{q}_i(t,z) \tag{5}$$

The *interstitial* gas velocity is related to the *superficial* gas velocity by

$$v = \frac{u}{\varepsilon} \tag{6}$$

In industrial practice, the most common operation uses a step-wise input of mixtures to be separated into an adsorber bed that is initially free of adsorbates, i.e. we have the initial condition

$$t = 0; \quad q_i(0,z) = 0 \tag{7}$$

At time, t = 0, the inlet to the adsorber, z = 0, is subjected to a step input of the n-component gas mixture and this step input is maintained till the end of the adsorption cycle when steady-state conditions are reached.

$$t \geq 0; \quad p_i(0,t) = p_{i0}; \quad u(0,t) = u_0 \tag{8}$$

where u_0 is the superficial gas velocity at the inlet to the adsorber.

The breakthrough characteristics for any component is essentially dictated by two sets of parameters: (a) The characteristic contact time $\frac{L}{v} = \frac{L\varepsilon}{u}$ between the crystallites and the surrounding fluid phase, and (b) $\frac{Đ_i}{r_c^2}$, that reflect the importance of intra-crystalline diffusion limitations. It is common to use the dimensionless time, $\tau = \frac{tu}{L\varepsilon}$, obtained by dividing the actual time, t, by the characteristic time, $\frac{L\varepsilon}{u}$ when plotting simulated breakthrough curves [4].

If the value of $\frac{Đ_i}{r_c^2}$ is large enough to ensure that intra-crystalline gradients are absent and the entire crystallite particle can be considered to be in thermodynamic equilibrium with the surrounding bulk gas phase at that time *t*, and position *z* of the adsorber

$$\bar{q}_i(t,z) = q_i(t,z) \tag{9}$$

The molar loadings at the *outer surface* of the crystallites, i.e. at $r = r_c$, are calculated on the basis of adsorption equilibrium with the bulk gas phase partial pressures p_i at that position *z* and time *t*. The adsorption equilibrium can be calculated on the basis of the IAST. The assumption of thermodynamic equilibrium at every position *z*, and any time *t*, i.e. invoking Equation (5), generally results in sharp breakthroughs for each component. Sharp breakthroughs are desirable in practice because this would result in high productivity of pure products. Essentially, the influence of intra-crystalline diffusion is to reduce the productivity of pure gases. For all the breakthrough calculations reported in this work, we assume negligible diffusion resistances for all materials and we invoke the simplified Equation (5).

Notation

b	Langmuir-Freundlich constant for species i at adsorption site A, $\mathrm{Pa}^{-\nu_i}$
c_i	molar concentration of species i in gas mixture, mol m^{-3}
c_{i0}	molar concentration of species i in gas mixture at inlet to adsorber, $molm^{-3}$
E	energy parameter, J mol^{-1}
L	length of packed bed adsorber, m
N_i	molar flux of species i, mol m^{-2} s^{-1}
p_i	partial pressure of species i in mixture, Pa
p_t	total system pressure, Pa
q_i	component molar loading of species i, mol kg^{-1}
$\bar{q}_i(t)$	spatially averaged component molar loading of species i, mol kg^{-1}
Q_{st}	isosteric heat of adsorption, J mol^{-1}
r_c	radius of crystallite, m
R	gas constant, 8.314 J mol^{-1} K^{-1}
t	time, s
T	absolute temperature, K
u	superficial gas velocity in packed bed, m s^{-1}
v	interstitial gas velocity in packed bed, m s^{-1}

Greek letters

ε	voidage of packed bed, dimensionless
ρ	framework density, kg m^{-3}
τ	time, dimensionless

Reference

[1]. Myers, A. L.; Prausnitz, J. M. Thermodynamics of mixed gas adsorption, A.I.Ch.E.J. 1965, 11, 121-130.

[2]. Myers AL. Equation of state for adsorption of gases and their mixtures in porous materials. Adsorption. 2003 Mar;9(1):9-16.

[3]. Yang JF, Li JM, Wang W, Li LB, Li JP. Adsorption of CO2, CH4, and N-2 on 8-, 10-, and 12-Membered Ring Hydrophobic Microporous High-Silica Zeolites: DDR, Silicalite-1, and Beta. Ind Eng Chem Res. 2013 Dec 18;52(50):17856-64.

[4]. Krishna R, Long JR. Screening metal-organic frameworks by analysis of transient breakthrough of gas mixtures in a fixed bed adsorber. J Phys Chem C. 2011;115:12941-50.

[5]. Krishna R. The Maxwell-Stefan Description of Mixture Diffusion in Nanoporous Crystalline Materials. Microporous Mesoporous Mater. 2014;185:30-50.

[6]. Krishna R, Baur R. Modelling issues in zeolite based separation processes. Sep Purif Technol. 2003;33:213-54.